communications physics

Article

https://doi.org/10.1038/s42005-024-01607-8

Rotation in attosecond vibronic coherence spectroscopy for molecules

Chi-Hong Yuen ✉ & Chii-Dong Lin

Excitation or ionization of a molecule by ultrafast laser pulses can create a superposition of electronic states, whose dynamics is influenced by the interplay of electronic coherence and nuclear motion, resulting in charge migration and possibly charge transfer. Probing the vibronic coherence is therefore vital to monitoring electronic dynamics and controlling chemical reactivity, as recently demonstrated in molecules via attosecond transient absorption spectroscopy (ATAS). However, theories supporting the interpretation of ATAS experiments neglect the effects of molecular rotation, often leading to inaccurate interpretation of experimental data. Here, we develop a comprehensive theory for ATAS of molecules encompassing the entire pump-probe process. Applying the theory to N_2, we demonstrate that the emergence of coherent signals critically depends on the consideration of molecular rotation. This work contributes to close the gap between theory and ATAS experiments, paving the way for monitoring electronic motion and controlling chemical reactivity in diverse molecular systems.

Coherence is a fundamental yet elusive quantity in quantum mechanics. Its survival gives rise to interference between quantum states, leading to intriguing phenomena in both atoms[1,2] and molecules[3–5]. Conversely, the loss of coherence due to other degrees of freedom can lead to intramolecular charge transfer, and remarkably, it can enhance energy transfer in photosynthesis[6]. While measuring coherence is of paramount importance, experiments can measure only the population of quantum states. Therefore, the measurement process generating the population must inherently rely on coherence, which often manifests as oscillatory signals in observables. However, in ultrafast spectroscopy, these oscillatory signals can have various origins due to the coherence of the laser pulses used. To understand the observed features in experiments, full quantum simulations become indispensable. The search for suitable measurement processes for coherence in different quantum systems under different scenarios thus becomes a tremendously challenging task.

The capability to monitor vibronic coherence in molecules stands as the next milestone in attosecond science. When a molecule is exposed to an intense ultrashort laser pulse, a superposition of electronic states could be formed by excitation or ionization. The coherence between them leads to an oscillatory behavior known as the quantum beat, driving attosecond (10^{-18} s) electronic motion throughout the molecular framework. This kind of electronic motion is termed charge migration[7–9]. However, the presence of nuclear degrees of freedom within molecules triggers vibrational dynamics within a few femtoseconds (1 fs = 10^{-15} s). As vibrational dynamics vary for different electronic states, vibronic coherence between these states could undergo rapid changes, and in some cases, it could even vanish. The vanishing of vibronic coherence has the potential to halt charge migration and result in permanent charge transfer, reshaping the chemical reactivity of a molecule[10,11]. Consequently, monitoring the vibronic coherence enables real-time observation of electronic motion and also holds the potential to control chemical reactivity, aligning with the ultimate goals of attosecond science[12].

So far, two promising pump–probe schemes for vibronic coherence have been simulated: dissociative sequential double ionization (DSDI)[13] and attosecond transient absorption spectroscopy (ATAS)[14–16]. In DSDI, a neutral molecule is first ionized by either a few-cycle infrared (IR) pulse or a short extreme ultraviolet (XUV) pulse to form a superposition of ionic states. At a later time, a few-cycle intense IR pulse further ionizes the pumped states to form dissociative dications. Since this process is partly driven by laser couplings[17,18], changes in vibronic coherence between the pumped states lead to changes in the dication yields, thereby imprinting the coherence to observables such as the kinetic energy release spectrum. There is theoretical evidence for this pump–probe scheme[13], and experimental verification is currently in progress. On the other hand, in ATAS, a neutral target is typically ionized by a few-cycle IR pulse and then probed using the absorption of an attosecond XUV or soft X-ray (SXR) pulse. While an attosecond XUV pulse can also generate the superposition of ionic states, it is not employed as the pump since achieving a sufficient signal-to-noise ratio in ATAS experiments is

J. R. Macdonald Laboratory, Department of Physics, Kansas State University, Manhattan, KS 66506, USA.
✉e-mail: iyuen@phys.ksu.edu

challenging due to the low photon flux. ATAS is widely considered a superior technique since it has excellent time resolution and can selectively probe specific atoms in a molecule when an SXR pulse is used. It has been shown that ATAS can probe the electronic coherence in atomic ions[1] and vibronic coherence in halogen-containing molecular ions[14,19]. The decoherence and revival in charge migration in the excited silane molecule were also observed using ATAS[5], making it a promising pump–probe scheme for charge migration or transfer.

Despite the tremendous experimental progress in ATAS, there is a significant knowledge gap in the theory: rotation of the molecule has not been considered. Rotational motion in a molecule occurs on the picosecond scale (10^{-12} s). Therefore, in femtosecond vibronic dynamics, rotation is negligible, and we can regard the molecular orientation as fixed. Additionally, since molecular orientation is isotropic in free space, it is reasonable to assume a fixed and uniform orientation to account for rotation during vibronic dynamics. However, the existing ATAS theories for molecules[14–16] have been directly derived from the theory for atoms[20], such that molecular orientation has been neglected. Particularly, the sudden ionization approximation, which assumes the population and coherence in the molecular ion are isotropic, has been routinely used to describe the interaction between the molecule and the intense pump laser pulse[5,14–16,21,22]. The primary rationale for employing this approximation is the inadequacy of perturbation theory and the high computational cost associated with first-principles approaches in describing strong field processes. As strong field interactions exhibit high anisotropy with respect to molecular orientation, such oversimplification can lead to distinct qualitative behaviors in simulated observables, posing challenges in accurately interpreting experimental data and extracting information about vibronic coherence.

In this article, we introduce a comprehensive theory capable of fully describing the anisotropy of the population and coherence created by the intense few-cycle IR pump pulse and simulating the resulting ATAS signals. Applying this theory to N_2, we highlight the crucial role that molecular orientation plays in uncovering distinctive signatures of vibronic coherence between the $A^2\Pi_u$ and $B^2\Sigma_u^+$ states of N_2^+ within the ATAS signal. To assess the applicability of ATAS for probing vibronic coherence in various molecules, we introduce a parameter called the coherence contrast factor (CCF), derived from orientation-dependent population and coherence. While the role of molecular orientation has been investigated[22], our focus here is on the anisotropy generated by the intense pump pulse in the target molecule.

Results

A key component of the current theory is a density matrix approach describing the interaction of the molecule with the intense few-cycle IR pump pulse at different orientations[23]. The diagonal and off-diagonal density matrix elements represent the population of the electronic states and the coherence between them. The IR pump pulse is strong enough to distort the Coulomb potential to tunnel ionize an electron from outer-valence orbitals of the neutral molecule, forming a superposition of ionic states. Simultaneously, the pump pulse also couples different electronic states of the nascent molecular ion. If the pulse duration is comparable to the vibrational period, nuclear dynamics and ionization dynamics can occur concurrently. Therefore, the laser-molecule interaction is highly complicated. To make the theory tractable, we consider two simplifications in our approach: (1) Nuclei of the molecule are frozen in the presence of a few-cycle IR pulse. (2) The ionized electron is neglected, making the residual ion an open system. The first simplification is justified when the duration of the IR pulse is much less than the vibrational period of the molecule. Consequently, the equation of motion for density matrices $\rho^{(q)}$ ($q = 0, 1$ for neutral or ionic states) are

$$\frac{d}{dt}\rho^{(q)}(t) = -\frac{i}{\hbar}[H^{(q)}(t), \rho^{(q)}(t)] + \Gamma^{(q)}(t), \tag{1}$$

with the ionization matrix

$$\Gamma^{(0)}(t) = -\sum_i \rho^{(0)}(t) W_i^{(0)},$$
$$\Gamma_{ij}^{(1)}(t) = \rho^{(0)}(t) \sum_m \gamma_{im}^{(0)}(t) \gamma_{jm}^{(0)^*}(t).$$

In the above, the density matrix ρ is represented in terms of electronic states of each charge state and $H^{(q)}$ is the Hamiltonian with the field-free term and the laser coupling term $-\mathbf{d}\cdot\mathbf{E}$. The equation for the neutral describes the depletion of population by tunnel ionization, where the rate $W_i^{(0)}$ to the ith ionic state is given by the molecular Ammosov–Delone–Krainov (MOADK) theory[24]. The equation for the ion simultaneously describes population and coherence build-up from multi-orbital tunnel ionization of the neutral and the laser couplings between nascent ionic states. To model the coherence build-up between the ith and jth ionic states from tunnel ionization, we trace out their MOADK ionization amplitudes $\gamma_{im}^{(0)}\gamma_{jm}^{(0)^*}$ over the magnetic quantum number m, which is approximately equivalent to tracing out all quantum numbers of the tunnel ionized electron[23]. For $i = j$, the term $\sum_m |\gamma_{im}^{(0)}|^2$ is simply the ionization rate $W_i^{(0)}$. Solving the above equations then yields the density matrix of the neutral and the ion at different orientations $\mathcal{R}$, thus fully accounting for the rotation of the molecule. The full-density matrix ρ is assumed to be block-diagonal for different charge states. Therefore, to construct ρ, we simply place $\rho^{(0)}$ and $\rho^{(1)}$ onto its diagonal.

During the time delay between the pump and probe pulses, the nuclear motion of the ion sets in. Assuming the laser-molecule interaction is approximately the same near the equilibrium geometry of the neutral molecule, the population of each vibronic state of the ion is proportional to the square of the spatial overlap of its wave function with the wave function of the neutral vibronic ground state. A nuclear wave packet $|\chi_i\rangle$ is then formed for each ionic state i. The vibronic coherence concerned here is the residual electronic coherence after tracing out the nuclear degrees of freedom. Therefore, the vibronic coherence between the ith and jth ionic states is proportional to the spatial overlap of their nuclear wave packets, $\langle\chi_j|\chi_i\rangle$. Its evolution during the pump–probe delay can be expressed as[13]

$$\rho_{ij}^{(1)}(\mathcal{R}, t) = C_{ij}(\mathcal{R})\langle\chi_j(t - t_1)|\chi_i(t - t_1)\rangle, \tag{2}$$

where $C_{ij}(\mathcal{R})$ matches the density matrix when the pump pulse ends at $t = t_1$ at each orientation $\mathcal{R}$. It follows that the population of the ith ionic state is constant during the pump-probe delay if the norm $\langle\chi_i|\chi_i\rangle$ remains unity.

A notable advantage of the current approach for describing the dynamics before the probe pulse is that it can be seamlessly adapted to large molecules. The key lies in using a few-cycle IR pump pulse, such that nuclei can be viewed as frozen during the laser-molecule interaction. This allows the nuclear dynamics to be treated by conventional quantum chemistry techniques with no external field at a fixed orientation[25–27].

An advance in this work is the extension of the ATAS theory to molecules at different orientations. The experimental observable in ATAS is the optical density (OD), which is proportional to the photoabsorption cross section $\sigma^{(1)}(\omega) = 4\pi\omega\mathrm{Im}[\chi^{(1)}(\omega)]/(nc)$, with ω being the probe frequency, n being the number density of the gas, and $\chi^{(1)}$ being the linear susceptibility[20]. Apart from the orientation dependence of the density matrix, the major difference in the theory for the atomic and molecular case is that the transition dipole moments (TDM) of the molecule must be transformed from the molecular frame to the laboratory frame. In Methods, we build upon the results of the atomic case[20] to derive the expression for the

orientation-averaged linear susceptibility for randomly oriented molecules,

$$\langle\chi^{(1)}\rangle(\omega,\Delta t)=\sum_{ij}\sum_{f}\sum_{\mu,\nu}\frac{d^{*}_{fj,\nu}d_{fi,\mu}\lambda_{ij;\nu\mu}(\Delta t)}{E_f-E_i-\omega-i\epsilon},$$
$$\lambda_{ij;\nu\mu}(\Delta t)=\frac{1}{4\pi}\int_0^{2\pi}\int_0^{\pi}\rho_{ij}(\Delta t,\beta,\gamma)\left[D^{1}_{0\nu}(0,\beta,\gamma)\right]^{*}D^{1}_{0\mu}(0,\beta,\gamma)\sin\beta d\beta d\gamma, \quad (3)$$

where D is the Wigner D-matrix and (β,γ) are the Euler angles. The Euler angle α is zero due to the use of linearly polarized laser fields. The full density matrix ρ_{ij}, obtained from Eqs. (1) and (2) depend on the pump–probe delays Δt as well as the Euler angles. $d_{fi,\mu}$ is the μ spherical component of the TDM between the final state f and the valence state i in the molecular frame, and E_f and E_i are their respective electronic energy. Finally, ϵ accounts for the resolution in the photon energy of a spectrometer. Since the diagonal and off-diagonal density matrix elements represent the population and coherence, the signals that arise from ρ_{ii} and ρ_{ij} are referred to as incoherent and coherent signals, respectively.

If the orientation dependence of the density matrix is neglected as in refs. 14–16, Eq. (3) reduces to (see Methods for details)

$$\langle\chi^{(1)}\rangle(\omega,\Delta t)=\frac{1}{3}\sum_{ij}\rho_{ij}(\Delta t)\sum_{f}\frac{\sum_{\mu}d^{*}_{fj,\mu}d_{fi,\mu}}{E_f-E_i-\omega-i\epsilon}. \quad (4)$$

This implies that coherence between states i and j can contribute to the overall signal only if the dot product of their TDM to state f is non-zero. Consequently, Eq. (4) suggests that signal from the coherence between a Σ and a Π state of a linear molecule vanishes, as their TDMs to state f must be perpendicular. This is in sharp contrast with the prediction from Eq. (3), in which the coherent signal can be non-vanishing due to the orientation dependence of the density matrix.

We observe that, in Eq. (3), coherence between states i and j can be probed only if both states can reach the same final state f. It implies that only coherence between electronic states with the same parity can be probed for molecules possessing inversion symmetry. It is opposite to the case of using the DSDI to probe vibronic coherence[13]. Since its probing mechanism relies on laser coupling between states i and j, the coherence signal is strong only if the two states have the opposite parity. As a result, ATAS and DSDI could be used synergistically to fully characterize vibronic coherence in molecules with inversion symmetry.

We now apply our ATAS theory to N_2. The probe pulse is assumed to be a high-harmonic generated isolated attosecond SXR pulse that covers the nitrogen K-edge. To create such a pulse, the typical required wavelength of the driving laser is about 1.8 μm. To ensure the pump and the probe pulse are phase-locked, we choose the pump pulse to be a linearly polarized Gaussian pulse, with 10 fs pulse duration, 1.8 μm central wavelength, and a peak intensity of 3×10^{14} W cm^{-2}. Note that the vibrational period of N_2 is about 13 fs such that nuclear motion may play a role during the ionization dynamics. Extension of the current framework to account for nuclear motion is reserved for future studies. The pump pulse populates the $X^2\Sigma_g^+$ ($3\sigma_g^{-1}$, 15.6 eV), $A^2\Pi_{u\pm}$ ($1\pi_u^{-1}$, 16.9 eV), and $B^2\Sigma_u^+$ ($2\sigma_u^{-1}$, 18.8 eV) states of N_2^+ from the $X^1\Sigma_g^+(\ldots2\sigma_u^2 1\pi_u^4 3\sigma_g^2)$ state of N_2. For brevity in the discussion, we refer to the neutral state as the $\tilde{X}$ state and the ionic states as the X, $A_{\pm}$, and B states hereafter. After the tunnel ionization, the X and $A_{\pm}$ states and the X and B states are coupled by the pump pulse. The evolution of the population of the X, $A_{\pm}$, and B states and the coherence between them are then further driven by the laser couplings. By solving Eq. (1), we obtain the density matrix of the neutral and the ion after the pump pulse at each molecular orientation. During the pump-probe delay, the nuclear wave packet for the ith electronic state evolves as $|\chi_i(t)\rangle=\sum_v|c_{iv}|e^{-iE_{iv}t}|\phi_{iv}\rangle$, where the Franck-Condon factors $|c_{iv}|^2$ and vibronic energies E_{iv} are given by ref. 28, and $|\phi_{iv}\rangle$ is the vibronic wave function. The vibronic coherence in the ion then evolves according to Eq. (2), while the population of the neutral and the ion remain constant in time. For the simulation of the OD from the probe pulse, we have included the following absorption lines: from $\tilde{X}$ to $1\sigma_u^{-1}1\pi_g^1$ (401 eV), from X to $1\sigma_u^{-1}3\sigma_g^{-1}1\pi_g^1$ (402, 403 eV), from X to $1\sigma_u^{-1}$ (393.5 eV), from A to $1\sigma_g^{-1}$(392 eV), and from B to $1\sigma_g^{-1}$ (391 eV) (see Methods for details).

A similar ATAS experiment for N_2 has been reported by Kleine et al.[21]. However, the IR pump pulse they employed has a central wavelength of 800 nm and a pulse duration of 50 fs. Since their IR pulse duration is long, nuclear motion cannot be neglected during the laser interaction, such that the molecular dynamics they considered significantly differ from this study. Furthermore, the SXR pulse they used has a pulse duration of 25 fs, making the short pulse approximation $E(t)\sim\delta(t)$ assumed in Eq. (3) to be invalid. Therefore, the dynamics induced by the probe pulse in ref. 21 also differ from those in this study. Nevertheless, for consistency and reference, we adopted the energies and TDMs for the transitions from ref. 21. We also used the same spectral resolution $\epsilon=\omega/890$ eV as in ref. 21.

We shall first examine the orientation dependence of the relevant density matrix elements. Figure 1a–d displays the population of the $\tilde{X}, X, A_{\pm}$, and B states over different angles β (γ is set to zero for linear molecules). It is clear that the populations of these states are anisotropic. The orientation-averaged population of the $\tilde{X}, X, A_{+}$, and B states is 0.44, 0.22, 0.11, and 0.12, respectively, such that one would expect the incoherent signal from the B state to be weaker. Since ATAS can only probe the coherence between the A and B states due to the restriction in parity, the density matrix element ρ_{AB} is of particular interest. Figure 1e shows the real part of ρ_{A_+B} at different orientations after the pump pulse. One can see that ρ_{A_+B} is an odd function and is highly anisotropic, such that according to Eq. (3), the coherence signal between the $A_{\pm}$ and B states can be non-vanishing. Figure 1f displays the degree of coherence (DOC) defined by $g_{A_+B}=|\rho_{A_+B}|/\sqrt{\rho_{A_+A_+}\rho_{BB}}$. The DOC takes values ranging from 0 to 0.65 at different orientations. Therefore, while the DOC serves as a useful indicator for the modulation in OD for atoms[1,29], it is less informative for molecules, and an orientation-averaged indicator is needed.

In the ATAS simulation, we assume that the pump pulse and the probe pulse do not overlap, such that the considered minimum time delay between the pulses is 10 fs. The absorption spectrum (ΔOD), which is the pump-probe OD subtracted by the probe-only OD at 10 fs time delay, is shown as the solid line in Fig. 2a. The strong bleach of the signal at 401 eV is due to the depletion of the $\tilde{X}$ state. Because the relative ratios for the oscillator strength are 0.8:1.0:0.15 for the X to $1\sigma_u^{-1}$, A to $1\sigma_g^{-1}$, and B to $1\sigma_g^{-1}$ transition[30], the relative intensity of their absorption lines scale differently than their populations.

The orientation-averaged absorption spectrum at different time delays is shown in Fig. 2b. In our simulation, only the off-diagonal density matrix elements vary over time delay [cf Eq. (2)]. As a result, signals from the incoherent terms, which come from the diagonal elements, are constant over the time delays. The absorption lines of the $\tilde{X}$ and X states are, therefore, constant in time. In contrast, due to the contribution from the ρ_{AB} term, there are modulations in the signal from the A and B states. However, the modulation is much weaker for the A state than the B state because the incoherent signal and the oscillator strength of the B state are only 15% of the A state, while the coherent signal is the same for both states.

To demonstrate the role of molecular orientations, in Fig. 2c, d, we compare the ATAS signal between 390 and 391 eV from Fig. 2b with the signal calculated using an isotropic density matrix. To have a fair comparison, we define the isotropic density matrix as the orientation-averaged of the anisotropic density matrix in Fig. 1. Since the orientation-averaged of ρ_{AB} is zero, we use its value at 60° for the isotropic density matrix. Both the anisotropic and isotropic signals are normalized to the same peak value. As anticipated, neglecting the rotation of the molecule leads to a complete disappearance of the coherent signal. This is because the TDM of the A and B states to the same core-hole state $1\sigma_g^{-1}$ are orthogonal to each other. It is also worth noting that the peak isotropic signal is roughly half the magnitude of the peak anisotropic signal, suggesting that the neglect of the rotation may

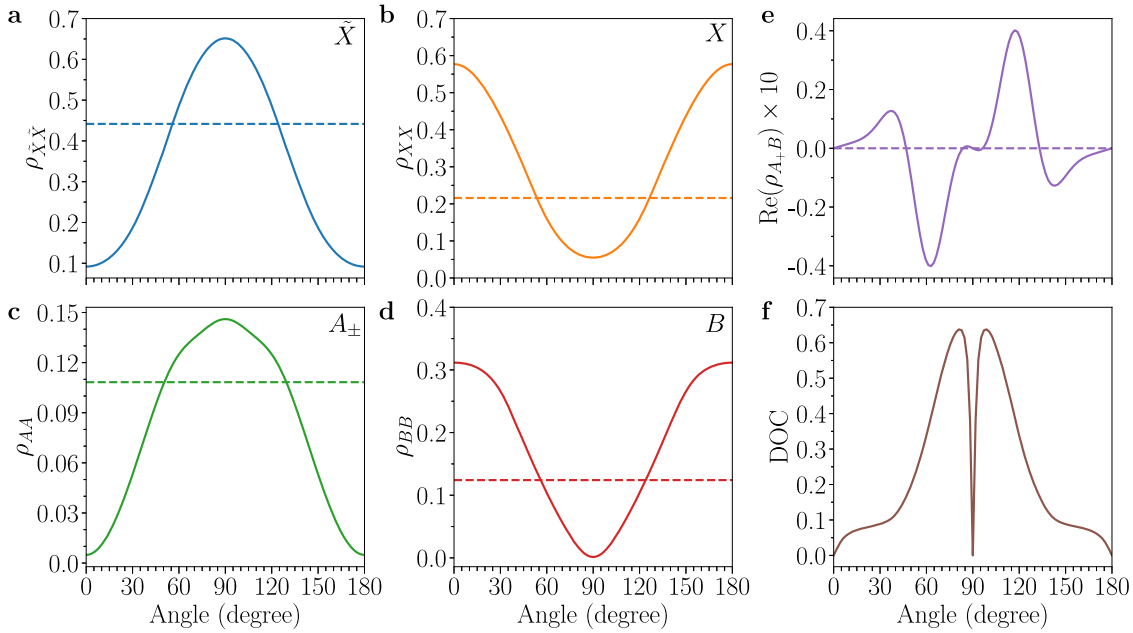

Fig. 1 | Orientation dependence of the relevant density matrix elements. a–d The population of the $\tilde{X}$ state of N_2, the X, $A_\pm$, and B states of N_2^+ at the end of the linearly polarized pump pulse with a 10 fs duration, 1.8 μm central wavelength, and peak intensity of 3×10^{14} W cm^{-2}. The dashed horizontal lines indicate their orientation averaged value. **e** The real part of the density matrix element ρ_{A_+B}. The orientation averaged value is zero since it is an odd function. **f** The degree of coherence (DOC) $g_{A_+B} = |\rho_{A_+B}|/\sqrt{\rho_{A_+A_+}\rho_{BB}}$. One can see that the population, coherence, and DOC vary greatly at different orientations.

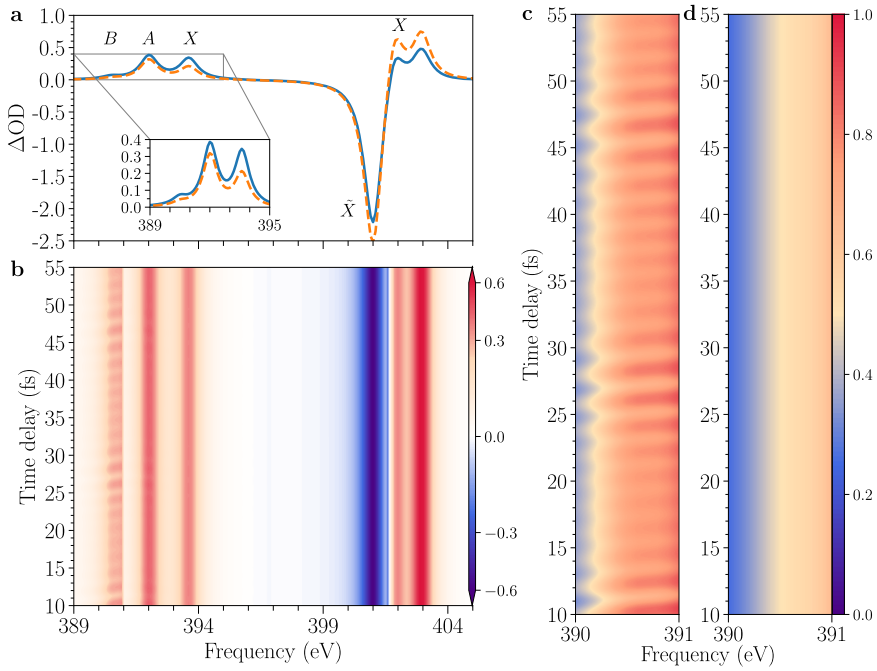

Fig. 2 | Simulated attosecond transient absorption spectra (ΔOD). a The pump–probe optical density (OD) subtracted by the probe-only OD, or ΔOD, at 10 fs time delay for the $\tilde{X}$ state of N_2 and the X, A, and B states of N_2^+. The spectra are calculated using the anisotropic (blue solid line, see Fig. 1) and isotropic (orange dashed line) density matrix, respectively. The inset shows the spectrum between 389 and 395 eV. One can see that the intensity of the signals differs significantly when the molecular orientation is neglected. **b** ΔOD calculated using the anisotropic density matrix at different time delays. To enhance the visual, the signal below 391 eV is enlarged by a factor of 4, and the signal between 397 and 401.5 eV is normalized to the positive maximum value. Modulation in the signal below 391 eV, which is due to the AB coherence, is clearly visible. **c**, **d** Comparison of ΔOD between 390 and 391 eV calculated using the anisotropic (**c**) or isotropic (**d**) density matrix. It is evident that neglecting the molecular orientation leads to a complete disappearance of the coherent signal.

impact the incoherent signals as well. To gain further insights, we include the absorption spectra with the isotropic density matrix at 10 fs time delay, represented as the dashed line in Fig. 2a. Comparing the absorption lines of the X state at 393.3 eV, we see that the result with the isotropic density matrix is about 40% weaker. Similarly, the absorption line of the A state shows a decrease of about 20% with the isotropic density matrix. As a result, neglecting the orientation dependence of the density matrix not only causes the disappearance of the coherent signals but also leads to noticeable changes in the incoherent signals. Figure 2 thus demonstrates that to accurately interpret the ATAS signal from experiments, the rotation of the molecule must be accounted for.

We can further analyze the modulation due to the coherent signal from the B and A states. In Fig. 3, we plot the integrated signal of the B state from 389 to 391 eV and of the A state from 391 to 393 eV in Fig. 2b. We see that the modulation exhibits clear dephasing and rephasing in a period of about 18 fs, which is roughly the return time for the A state nuclear wave packet to the equilibrium geometry of the neutral. The maximum trough-to-peak ratio of the signal from the B and A states due to the varying AB vibronic coherence is about 0.81 and 0.95, respectively. This ratio for the A state is close to one because the incoherent signal from the A state is much stronger than the B state. Therefore, the modulation in the B state signal should be distinguishable from the noise in experiments, while the modulation in the

A state signal is unlikely to be observed. To compare the qualitative behavior between ΔOD and vibronic coherence, the real part of the A_+B coherence $\mathrm{Re}(\rho_{A_+B})$ at 45° at different time delays is also shown in Fig. 3. This angle is chosen for the A_+B coherence as it mimics the effect of orientation averaging. We see that the integrated signal and the A_+B coherence follow the same qualitative behavior, such that the coherent signal indeed arises from the A_+B coherence. There is a small relative phase between the integrated signal and the A_+B coherence because the integrated signal is orientation averaged.

Discussion

To this end, it would be useful to define an orientation-averaged factor to quantify the robustness of ATAS for probing vibronic coherence in molecules. Using Eq. (3), we can define a coherence contrast factor (CCF) for the absorption line from the ith state to the f state,

$$\mathrm{CCF}_{fi} = \frac{\sum_{j\neq i}\sum_{\mu,\nu} d^*_{fj,\nu} d_{fi,\mu} \mathrm{Re}[\lambda_{ij;\nu\mu}(t_m)]}{\sum_{\mu,\nu} d^*_{fi,\nu} d_{fi,\mu} \mathrm{Re}(\lambda_{ii;\nu\mu})}, \tag{5}$$

where t_m is the time delay when $\lambda_{ij;\nu\mu}$ is maximum and is taken as 10 fs here. The trough-to-peak ratio of the signal is then given by $(1-\mathrm{CCF})/(1+\mathrm{CCF})$. If the CCF is small, then the contrast in the signal due to the coherence will be weak. For the absorption line of the B state and the A state, the CCF is 0.1 and 0.01, respectively. As a result, the predicted trough-to-peak ratio is about 0.82 and 0.98 for the B state and the A state, which agree quantitatively with Fig. 3. We note that the CCF can also be extracted from the trough-to-peak ratio measured in experiments to compare with theories.

To conclude, ATAS proves to be a robust method for probing vibronic coherence in molecules. The necessary and sufficient conditions for ATAS to detect vibronic coherence between two arbitrary quantum states (i and j) are as follows:

(i.) Both states i and j must reach the same final state f upon interaction with the attosecond probe pulse. This condition implies that, for molecules with inversion symmetry, ATAS can only probe coherence between states of the same parity. In addition, if states i and j have different electronic spin, ATAS can detect their coherence only if there are spin-orbit couplings.

(ii.) The coherence contrast factor for either state i or j should be sufficiently large to distinguish the modulation due to the variation of vibronic coherence from the signal noise. To verify whether this condition is satisfied, acquiring the density matrix of the pumped molecule at different molecular orientations and the TDMs $\mathbf{d}_{fi}$ and $\mathbf{d}_{fj}$ are necessary.

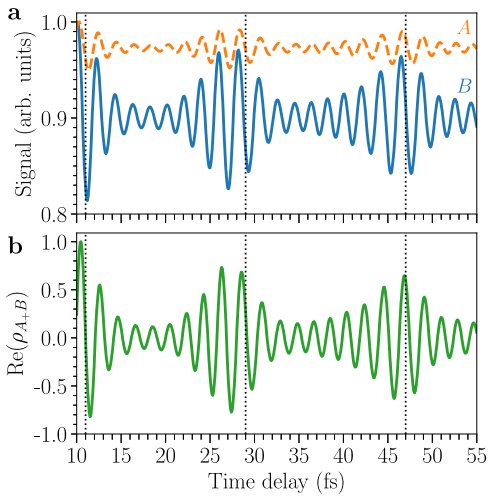

Fig. 3 | Comparison of ATAS trace with vibronic coherence. a Integrated signal of the B state from 389 to 391 eV (solid line) and of the A state from 391 to 393 eV (dashed line) in Fig. 2b, normalized to their respective peak values. The modulation in the A state signal is much weaker than in the B state because the incoherent signal of the A state is about 85% larger than the B state, while the coherent signal for both states is the same. The modulation shows a period of around 18 fs, indicated by the vertical dotted lines, corresponding to the return time of the A state nuclear wave packet to the equilibrium geometry of the neutral. **b** Real part of ρ_{A_+B} at 45° at different time delays, also normalized to the peak value. The modulation in the integrated signals follows the same qualitative behavior as the real part of ρ_{A_+B}, showing that the modulation indeed arises from the AB coherence.

With the robustness of ATAS being quantified, we anticipate it to be a useful approach for studying vibronic coherence in molecules. Another promising method with a solid theoretical foundation is the dissociative sequential double ionization [13]. The two methods could complement each other to provide a complete characterization of vibronic coherence in a pumped molecule. We eagerly anticipate future experimental validation of our predictions. With the necessary experimental techniques already well-established, the full realization of monitoring vibronic coherence in generic molecules is within reach in the near future.

Methods

Orientation averaging of the linear susceptibility

A full derivation of the formulas below can be found in Supplementary Notes 1 and 2. Here, we start from the expression of linear susceptibility $\chi^{(1)}$ for a fixed-in-space molecule with Euler angles (β,γ), which has a similar expression to Eq. (33) in ref. 20 and Eq. (2) in ref. 15,

$$\chi^{(1)}(\beta,\gamma,\omega,\Delta t) = \sum_{ij}\rho_{ij}(\beta,\gamma,\Delta t)\sum_f d_{jf,z}(\beta,\gamma)d_{fi,z}(\beta,\gamma)\left[\frac{1}{E_f - E_i - \omega - i\epsilon}\right]. \tag{6}$$

To obtain Eq. (3), we express the transition dipole moment (TDM) in the laboratory frame by

$$d_{fi,z}(\beta,\gamma) = \sum_{\mu=-1}^{1} d'_{fi,\mu} D^1_{0\mu}(0,\beta,\gamma), \tag{7}$$

where $d'_{fi,\mu}$ is the TDM in the molecular frame with $d'_{\pm} = (\mp d'_x + i d'_y)/\sqrt{2}$ and $d'_0 = d'_z$. Note that the above expression is independent of the Euler angle α due to the use of linearly polarized laser pulses. Substituting Eq. (7) in Eq. (6), and after integrating over β and γ and dividing by 4π, we arrive at Eq. (3).

If the density matrix ρ_{ij} is isotropic, then using the orthogonality of the Wigner D-matrix,

$$\int_0^{2\pi}\int_0^{\pi} \left[D^1_{0\nu}(0,\beta,\gamma)\right]^* D^1_{0\mu}(0,\beta,\gamma)\sin\beta d\beta d\gamma = \frac{4\pi}{3}\delta_{\nu\mu},$$

we arrive Eq. (4).

Table 1 | Core-valence transition energies and dipole moments of N_2 and N_2^+

Initial state	Final state	Energy (eV)	Dipole moment (a.u.)
N_2 ($\tilde{X}^1\Sigma_g^+$)	$1\sigma_u^{-1}1\pi_g$	401.0	$9.20\times10^{-2}\hat{x}$
N_2^+ ($X^2\Sigma_g^+$)	$1\sigma_u^{-1}$	393.6	$5.54\times10^{-2}\hat{z}$
N_2^+ ($X^2\Sigma_g^+$)	$1\sigma_u^{-1}3\sigma_g^{-1}1\pi_g$	401.8	$9.19\times10^{-2}\hat{x}$
N_2^+ ($X^2\Sigma_g^+$)	$1\sigma_u^{-1}3\sigma_g^{-1}1\pi_g$	402.9	$7.59\times10^{-2}\hat{x}$
N_2^+ ($A^2\Pi_u$)	$1\sigma_g^{-1}$	392.0	$6.92\times10^{-2}\hat{x}$
N_2^+ ($B^2\Sigma_u^+$)	$1\sigma_g^{-1}$	390.5	$2.40\times10^{-2}\hat{z}$

Core-valence transition dipole moments

The TDMs of N_2^+ ($X^2\Sigma_g$) are obtained from ref. 31. The TDM of N_2 ($\tilde{X}^1\Sigma_g^+$) was obtained by assuming the oscillator strength is the same for $X^2\Sigma_g^+$ to $1\sigma_u^{-1}3\sigma_g^{-1}1\pi_g$. The TDMs of N_2^+ ($A^2\Pi_u$) and N_2^+ ($B^2\Sigma_u^+$) are obtained by using the oscillator strength ratio 0.8: 1.0: 0.15 for the X to $1\sigma_u^{-1}$, A to $1\sigma_g^{-1}$, and B to $1\sigma_g^{-1}$ transition[30]. Table 1 shows the transition energies and TDMs used in this work.

Data availability

All relevant data presented in the paper are available upon reasonable request.

Code availability

The computer code used in the paper is available upon reasonable request.

Received: 27 December 2023; Accepted: 25 March 2024;
Published online: 04 April 2024

References

1. Goulielmakis, E. et al. Real-time observation of valence electron motion. *Nature* **466**, 739–743 (2010).
2. Nandi, S. et al. Observation of rabi dynamics with a short-wavelength free-electron laser. *Nature* **608**, 488–493 (2022).
3. Calegari, F. et al. Ultrafast electron dynamics in phenylalanine initiated by attosecond pulses. *Science* **346**, 336–339 (2014).
4. Li, S. et al. Attosecond coherent electron motion in Auger-Meitner decay. *Science* **375**, 285–290 (2022).
5. Matselyukh, D. T., Despré, V., Golubev, N. V., Kuleff, A. I. & Wörner, H. J. Decoherence and revival in attosecond charge migration driven by non-adiabatic dynamics. *Nat. Phys.* **18**, 1206–1213 (2022).
6. Cao, J. et al. Quantum biology revisited. *Sci. Adv.* **6**, eaaz4888 (2020).
7. Cederbaum, L. S. & Zobeley, J. Ultrafast charge migration by electron correlation. *Chem. Phys. Lett.* **307**, 205–210 (1999).
8. Remacle, F. & Levine, R. D. An electronic time scale in chemistry. *Proc. Natl Acad. Sci. USA* **103**, 6793–6798 (2006).
9. Folorunso, A. S. et al. Molecular modes of attosecond charge migration. *Phys. Rev. Lett.* **126**, 133002 (2021).
10. Remacle, F., Levine, R. & Ratner, M. Charge directed reactivity: a simple electronic model, exhibiting site selectivity, for the dissociation of ions. *Chem. Phys. Lett.* **285**, 25–33 (1998).
11. Lépine, F., Ivanov, M. Y. & Vrakking, M. J. Attosecond molecular dynamics: fact or fiction? *Nat. Photonics* **8**, 195–204 (2014).
12. Biegert, J., Calegari, F., Dudovich, N., Quéré, F. & Vrakking, M. Attosecond technology (ies) and science. *J. Phys. B* **54**, 070201 (2021).
13. Yuen, C. H. & Lin, C. D. Probing vibronic coherence in charge migration in molecules using strong-field sequential double ionization. *Phys. Rev. A* **109**, L011101 (2024).
14. Kobayashi, Y. et al. Coherent electronic-vibrational dynamics in deuterium bromide probed via attosecond transient-absorption spectroscopy. *Phys. Rev. A* **101**, 063414 (2020).
15. Golubev, N. V., Vaníček, J. & Kuleff, A. I. Core-valence attosecond transient absorption spectroscopy of polyatomic molecules. *Phys. Rev. Lett.* **127**, 123001 (2021).
16. Kobayashi, Y., Neumark, D. M. & Leone, S. R. Theoretical analysis of the role of complex transition dipole phase in XUV transient-absorption probing of charge migration. *Opt. Express* **30**, 5673–5682 (2022).
17. Yuen, C. H. & Lin, C. D. Density-matrix approach for sequential dissociative double ionization of molecules. *Phys. Rev. A* **106**, 023120 (2022).
18. Yuen, C. H., Modak, P., Song, Y., Zhao, S.-F. & Lin, C. D. Modeling the sequential dissociative double ionization of O_2 by ultrashort intense infrared laser pulses. *Phys. Rev. A* **107**, 013112 (2023).
19. Kobayashi, Y., Neumark, D. M. & Leone, S. R. Attosecond XUV probing of vibronic quantum superpositions in Br_2^+. *Phys. Rev. A* **102**, 051102(R) (2020).
20. Santra, R., Yakovlev, V. S., Pfeifer, T. & Loh, Z.-H. Theory of attosecond transient absorption spectroscopy of strong-field-generated ions. *Phys. Rev. A* **83**, 033405 (2011).
21. Kleine, C. et al. Electronic state population dynamics upon ultrafast strong field ionization and fragmentation of molecular nitrogen. *Phys. Rev. Lett.* **129**, 123002 (2022).
22. Bouakline, F. & Saalfrank, P. Seemingly asymmetric atom-localized electronic densities following laser-dissociation of homonuclear diatomics. *J. Chem. Phys.* **154**, 234305 (2021).
23. Yuen, C. H. & Lin, C. D. Coherence from multiorbital tunneling ionization of molecules. *Phys. Rev. A* **108**, 023123 (2023).
24. Tong, X.-M., Zhao, Z. X. & Lin, C.-D. Theory of molecular tunneling ionization. *Phys. Rev. A* **66**, 033402 (2002).
25. Vacher, M., Bearpark, M. J., Robb, M. A. & Malhado, J. P. Electron dynamics upon ionization of polyatomic molecules: coupling to quantum nuclear motion and decoherence. *Phys. Rev. Lett.* **118**, 083001 (2017).
26. Arnold, C., Vendrell, O. & Santra, R. Electronic decoherence following photoionization: full quantum-dynamical treatment of the influence of nuclear motion. *Phys. Rev. A* **95**, 033425 (2017).
27. Golubev, N. V., Begušić, T. & Vaníček, J. On-the-fly ab initio semiclassical evaluation of electronic coherences in polyatomic molecules reveals a simple mechanism of decoherence. *Phys. Rev. Lett.* **125**, 083001 (2020).
28. Gilmore, F. R., Laher, R. R. & Espy, P. J. Franck–Condon factors, r-centroids, electronic transition moments, and Einstein coefficients for many nitrogen and oxygen band systems. *J. Phys. Chem. Ref. Data* **21**, 1005–1107 (1992).
29. Rohringer, N. & Santra, R. Multichannel coherence in strong-field ionization. *Phys. Rev. A* **79**, 053402 (2009).
30. Glans, P., Skytt, P., Gunnelin, K., Guo, J.-H. & Nordgren, J. Selectively excited X-ray emission spectra of N_2. *J. Electron Spectrosc. Relat. Phenom.* **82**, 193–201 (1996).
31. Lindblad, R. et al. X-ray absorption spectrum of the N_2^+ molecular ion. *Phys. Rev. Lett.* **124**, 203001 (2020).

Acknowledgements

The authors thank Meng Han for the helpful discussions. This work was supported by the Chemical Sciences, Geosciences and Biosciences Division, Office of Basic Energy Sciences, Office of Science, U.S. Department of Energy under Grant No. DE-FG02-86ER13491.

Author contributions

C.H.Y. conceived the research and performed all calculations. C.D.L. supervised the research. C.H.Y. and C.D.L. wrote the paper.

Competing interests

The authors declare no competing interests.

Additional information

Supplementary information The online version contains supplementary material available at https://doi.org/10.1038/s42005-024-01607-8.

Correspondence and requests for materials should be addressed to Chi-Hong Yuen.

Peer review information *Communications Physics* thanks Hongchuan Du and the other anonymous reviewer(s) for their contribution to the peer review of this work. A peer review file is available.